Pharm Res (2015) 32:321–336
DOI 10.1007/s11095-014-1466-4

RESEARCH PAPER

Development of a New Technique for the Efficient Delivery of Aerosolized Medications to Infants on Mechanical Ventilation

P. Worth Longest • Geng Tian

Received: 17 January 2014 / Accepted: 24 July 2014 / Published online: 8 August 2014

ABSTRACT

Purpose To evaluate the efficiency of a new technique for delivering aerosols to intubated infants that employs a new Y-connector, access port administration of a dry powder, and excipient enhanced growth (EEG) formulation particles that change size in the airways.

Methods A previously developed CFD model combined with algebraic correlations were used to predict delivery system and lung deposition of typical nebulized droplets (MMAD = 4.9 μm) and EEG dry powder aerosols. The delivery system consisted of a Y-connector [commercial (CM); streamlined (SL); or streamlined with access port (SL-port)] attached to a 4-mm diameter endotracheal tube leading to the airways of a 6-month-old infant.

Results Compared to the CM device and nebulized aerosol, the EEG approach with an initial 0.9 μm aerosol combined with the SL and SL-port geometries reduced device depositional losses by factors of 3-fold and >10-fold, respectively. With EEG powder aerosols, the SL geometry provided the maximum tracheobronchial deposition fraction (55.7%), whereas the SL-port geometry provided the maximum alveolar (67.6%) and total lung (95.7%) deposition fractions, respectively.

Conclusions Provided the aerosol can be administered in the first portion of the inspiration cycle, the proposed new method can significantly improve the deposition of pharmaceutical aerosols in the lungs of intubated infants.

P. W. Longest (✉) • G. Tian
Department of Mechanical and Nuclear Engineering, Virginia Commonwealth University, 401 West Main Street, P.O. Box 843015 Richmond, Virginia 23284-3015, USA
e-mail: pwlongest@vcu.edu

G. Tian
e-mail: tiang@mymail.vcu.edu

P. W. Longest
Department of Pharmaceutics, Virginia Commonwealth University Richmond, Virginia, USA

KEY WORDS active dry powder inhaler system · excipient enhanced growth (EEG) · neonate · pharmaceutical aerosols · streamlined Y-connector

ABBREVIATIONS

ACI	Andersen Cascade Impactor
AS	Albuterol sulfate
B#	Airway bifurcation number
CDC	Centers for Disease Control
CFD	Computational fluid dynamics
CM	Commercial
DE	Deposition efficiency
DF	Deposition fraction
ED	Emitted dose
EEG	Excipient enhanced growth
ETT	Endotracheal tube
FR	Fraction remaining
GSD	Geometric standard deviation
ID	Internal diameter
LL	Left lower (lung lobe)
LPM	Liters per minute
LRN	Low Reynolds number
MDI	Metered dose inhaler
MMAD	Mass median aerodynamic diameter
RH	Relative humidity
SIP	Stochastic individual path
SL	Streamlined
TB	Tracheobronchial

INTRODUCTION

Infants receiving mechanical ventilation with an endotracheal tube (ETT) may benefit from the delivery of a number of current and envisioned aerosolized medications (1–3). However, it is well known that current aerosol delivery systems

for administering medications to ventilated infants are highly inefficient (1,2,4,5). As a result, it is not clear if aerosolized medications that do not provide a clear clinical benefit to infants fail because of a lack of drug efficacy or poor drug delivery to the lungs (2). Improved aerosol delivery systems are needed so that drugs that are known to be effective, such as bronchodilators, can be delivered safely and at prescribed dosages to the airways of ventilated infants. Increasing delivery efficiency of aerosolized medications will also allow for the effective development of future therapies by providing controlled doses to the lungs in a reliable and reproducible manner.

Commonly used devices for delivering aerosolized medications to ventilated infants are jet nebulizers and metered dose inhalers (MDI). Challenges associated with aerosol delivery to the lungs of infants include low tidal volumes, short inhalation periods, high breathing frequencies (1,4), complex flow paths from the aerosol generator to the end of the ETT (6), and ETTs with very small internal diameters (3–4 mm) (7). Commercial nebulizers and MDIs, which are typically designed for delivering aerosols to adults, are often implemented for administering aerosol therapy to children. As a result, a majority of the drug dose intended for the pediatric airway is lost in the aerosol generation device, connective tubing, ventilator Y-connector, and ETT (1,2,7). For a jet nebulizer or MDI used to administer aerosols to premature infants, Fok *et al.* (5) reported <1% lung deposition fraction *in vivo*. These results are representative of delivery efficiencies for ventilated pediatric patients based on subsequent animal and *in vitro* models (1,2,8). *In vitro* model results tend to predict marginally higher lung delivery efficiencies compared with *in vivo* results due to a lack of a complete lung model, exclusion of the exhaled aerosol fraction, and sometimes the absence of airflow humidification (1,2). However, lung delivery efficiencies for jet nebulizers and MDIs based on *in vitro* models of ventilated infants still remain below approximately 10% and near 1%. It is noted that *in vitro* models typically evaluate lung delivery efficiency, which is the fraction of the initial aerosol reaching the lungs and is often captured on a filter. *In vivo* and some numerical models provide lung deposition fractions, which describe the fraction of the initial aerosol that enters the lungs and deposits.

It is often suggested that at an approximately 1% lung deposition fraction, an infant receives equal or more dose per kg of body weight of the aerosolized medication compared with an adult (1). A concern with this approach is that decreasing delivery efficiency is typically associated with increased dose variability. This inverse relationship has been proven for lung delivery of orally inhaled products (9), and is expected to also be true for aerosol delivery during mechanical ventilation due to a wide variety of available aerosol generation devices, ventilation circuits, ETT sizes, and ventilation parameters. Very low delivery efficiency along with high drug loss and high variability may be clinically acceptable for low dose medications with wide therapeutic windows and minor side effects. However, better control of inter- and intra-subject dose variability is likely required for the effective delivery of next generation inhaled medications, like non-steroidal anti-inflammatory medications, and medications with high required dosages, like inhaled antibiotics and surfactants.

Compared with other modes of aerosol generation, vibrating mesh nebulizers have demonstrated improved aerosol lung delivery efficiency based on infant models of mechanical ventilation (2,3,10). These nebulizers employ a vibrating mesh with apertures of a defined size and do not require additional airflow to form the droplets, thereby minimizing deposition in the ventilation system. The vibrating mesh nebulizer is typically attached to the ventilator inspiratory arm using a T-connector and delivers aerosol either continuously or synchronized with the inspiratory cycle. Using an infant ventilation model based on 2.6 kg macaques and a 3 mm (internal diameter; ID) ETT, Dubus *et al.* (11) demonstrated lung deposition fractions with continuous and synchronized mesh nebulizers of 12.6% and 14.0%, respectively, as a percentage of nebulizer charge. Sidler-Moix *et al.* (12) demonstrated a similar delivery efficiency using a mesh nebulizer in an *in vitro* model; however, continuous operation delivered 13.3% of the aerosol to the end of the ETT whereas synchronized operation delivered only 5.4%. In an *in vitro* study of adult and pediatric ventilation, Ari *et al.* (13) demonstrated that for pediatric patients, placement position of the nebulizer in the inspiratory arm of the ventilation circuit did not produce a statistical difference in aerosol delivery efficiency; however, a mesh nebulizer consistently delivered higher doses to the end of the ETT compared with a jet nebulizer. As a result of these studies with infant models, mesh nebulizers typically display the best performance of commercially available devices with lung delivery efficiencies for ventilated infants typically in the range of 10%.

Several advances have recently been reported for the delivery of aerosolized medications to infants. Mazela *et al.* (14) describes a newly designed Y-connector, referred to as the VC connector (also known as Afectair), that separates nebulizer and ventilation gas bias flows thereby improving the lung delivery efficiency of a jet nebulizer when used with infants. Based on an *in vitro* model of ventilated premature infants, Mazela *et al.* (14) reported delivery efficiency at the exit of a commercial Y-connector to be approximately 1% or less *vs.* a maximum of approximately 7% with the VC connector. Pohlmann *et al.* (15) developed an aerosol device for delivering high concentrations of a spray dried surfactant formulation to infants through a nasal cannula interface. The powder was aerosolized using a new pulsed air device, coated with water in a separate chamber, and then delivered to the patient interface. Pohlmann *et al.* (15) stressed that for high aerosol

doses delivered to infants, it is important for powders to have some water content prior to deposition to avoid airway injury. Delivery efficiency at the system outlet leading to an interface device, but not including the nasal prongs, was approximately 55% (15). The study of Laube *et al.* (16) is one of the first to describe the delivery of dry powder aerosols to infants. Powder aerosols were formed in a bag spacer and delivered to a nasal model of a 9 month old infant using a face mask. For an inhaled tidal volume of 100 ml, drug delivery to a filter at the end of the nasal model was 1.14% of the aerosol, which is representative of other tidal volume conditions. In adults, Everard *et al.* (17) developed a DPI system that delivered aerosols into a ventilation circuit and produced delivery efficiency at the end of a 9 mm ETT of approximately 20%.

In a previous study, Longest *et al.* (7) considered optimal aerosol delivery conditions for a newborn full-term infant receiving mechanical ventilation through an ETT using *in vitro*, CFD, and whole-lung modeling techniques. With a mesh nebulizer, commercial Y-connector, and a 3 mm ETT, the predicted lung deposition fraction was found to range from 6.8 to 13.5%, which was similar to the *in vivo* animal model predictions of Dubus *et al.* (11) with a lung deposition fraction range of 12.6–14%. Aerosol deposition in infant lungs was then optimized by Longest *et al.* (7) for mesh nebulizer aerosols with the use of a new streamlined (SL) Y-connector, delivery of the aerosol during the first half of inspiration, and selection of optimal droplet sizes from the aerosol generator. Lung deposition was shown to be a balance between selecting aerosols that were small enough to reduce deposition in the ventilator components and large enough to foster lung deposition. Optimal lung deposition was achieved with the streamlined Y-connector and synchronized delivery resulting in 45% and 60% lung deposition of polydisperse (MMAD ~ 1.8 μm) and monodisperse (~2.5 μm) droplets, respectively.

Based on the findings of Longest *et al.* (7), as well as the development of other recent technologies, it appears that the lung deposition efficiency of aerosols in ventilated infants can be further enhanced. In addition, the development of a dry powder delivery system for ventilated infants will be useful based on advantages associated with improved formulation stability, convenience, and low device cost. In developing a new dry powder delivery system, the use of the streamlined Y-connector of Longest *et al.* (7) should be retained. Compared with a commercial version, the streamlined Y-connector reduced aerosol loss in the Y-connector geometry by factors as large as 9-fold (7). The optimized delivery conditions developed in Longest *et al.* (7) were based on a fixed particle size analysis. In separate research, the concept of excipient enhanced growth (EEG) delivery has been described in which combination aerosol particles consist of a drug and hygroscopic excipient (18,19). These submicrometer combination particles minimize deposition in the delivery device and extrathoracic region (20–23). Size increase of the aerosol particles due hygroscopic growth in the respiratory airway humidity then ensures lung deposition and potential targeting of the site of drug delivery (24,25). As a novel method to further improve respiratory drug delivery to intubated infants, the EEG approach may provide the advantages of efficient lung delivery and potentially targeting the site of deposition within the airways. This approach will allow for the delivery of dry powder aerosols to infants on mechanical ventilation and ensure that the aerosols have a high water content before deposition, which will avoid exposing the airway surfaces to the direct deposition of dry particles.

The objective of this study is to evaluate the efficiency of a new technology for delivering aerosols to intubated infants that employs a new streamlined Y-connector, access port administration of a dry powder aerosol, and an EEG approach based on a previously tested CFD model that includes the ventilation circuit and extends through the conducting airways. For EEG delivery, initial aerosol particle sizes of 0.9 and 1.8 μm are considered consisting of a 50:50 by mass combination of albuterol sulfate (AS; as a model drug) and NaCl (as a hygroscopic excipient). The infant model is based on ventilation parameters and anatomy of a 6-month-old child intubated with a 4 mm ETT. Comparisons are made for the EEG delivery approach with the aerosol administered through a port on the SL Y-connector (port delivery) or with the aerosol administered in the ventilation circuit inspiratory line (line delivery). CFD simulations are conducted to evaluate aerosol transport, size change, and deposition in the ventilation delivery system, including the ETT, and throughout the conducting airways. A previously developed stochastic individual path (SIP) modeling approach is implemented to allow for CFD simulations of conducting airway transport through the 15th respiratory bifurcation of an infant.

MATERIALS AND METHODS

Aerosol Delivery Systems

In this study, three separate delivery systems are considered that represent a portion of the circuit employed for the mechanical ventilation of an approximately 6-month-old male infant. The systems include inspiratory and expiratory lines of tubing with 10 mm ID and lengths of 10 cm, a Y-connector, and an ETT with a 4 mm ID (Fig. 1). The ETT includes a 2.8 cm radius of curvature to represent passage through the oropharynx with the end of the ETT extending to the middle of the trachea. The three delivery systems considered differ based on the design of the Y-connector geometry and the administration method of the aerosol. The first system represents a control and consists of a commercial (CM) Y-connector (Teleflex Medical, Research Triangle Park, NC) with the

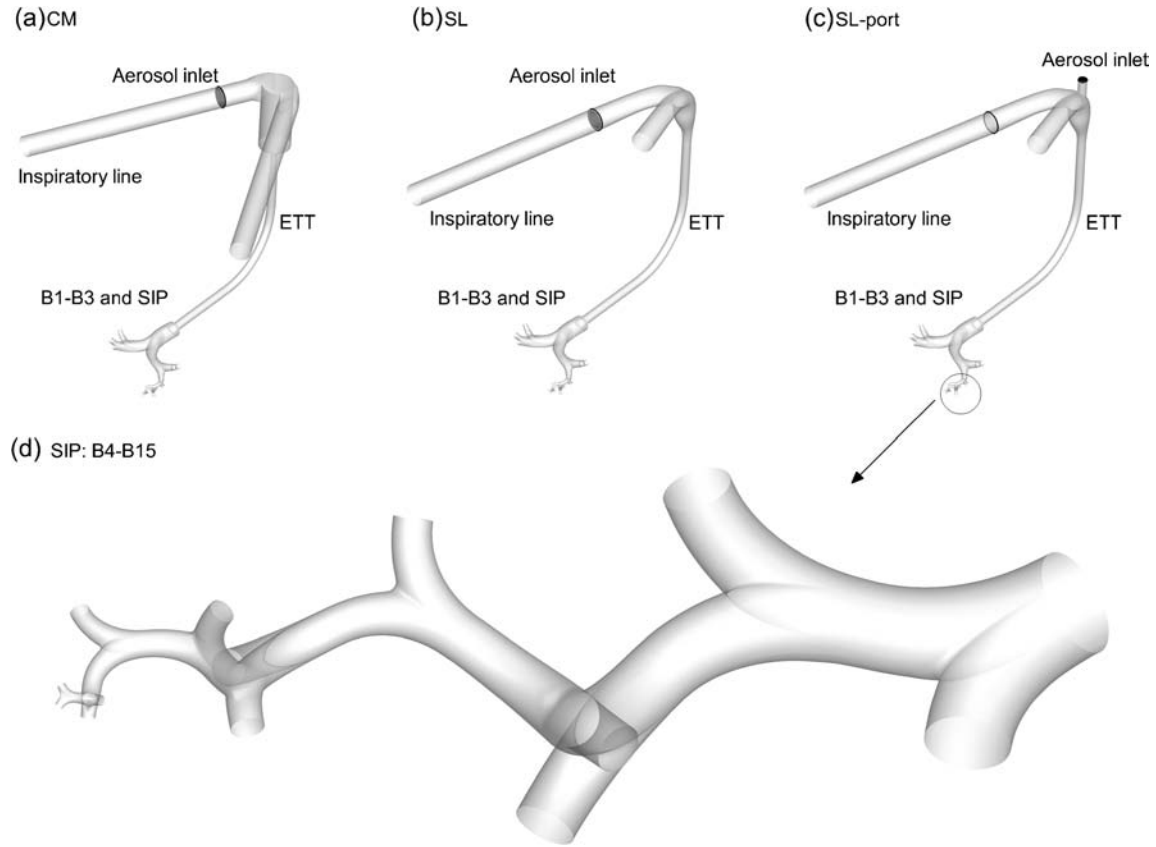

Fig. 1 Three delivery systems (**a**) commercial (*CM*), (**b**) streamlined (*SL*), and (**c**) streamlined with port (*SL-port*) are connected to an endotracheal tube (*ETT*) leading to the conducting airways; and (**d**) an expanded view of the stochastic individual path (*SIP*) model extending from the fourth bifurcation (*B4*) to the terminal bronchioles (*B15*) in the left lower (*LL*) lung lobe.

inspiratory and expiratory arms forming a 60° angle at the Y-connector (Fig. 1a). In this system, aerosol administration occurs in the inspiratory line at the inlet to the Y and is typically achieved with a T-connector, as presented and analyzed by Longest *et al.* (6,26). The second system consists of a newly designed streamlined (SL) Y-connector for adults (6) and pediatric patients (7). In the SL design, sharp changes in flow direction are replaced with more gradual changes (Fig. 1b). The centerline radius of curvature between the inspiratory/expiratory lines and ETT for the infant SL design is approximately 1 cm. The ETT is aligned with the end of the junction region opposite the inspiratory/expiratory lines (Fig. 1b), which is important to avoid further changing the direction of the gas flow as it enters the ETT. With this setup, the aerosol is again administered in the inspiratory line of the circuit at the inlet to the Y geometry. The division between the inspiratory arm and Y geometry is illustrated in Fig. 1 with a dark line. The third delivery system implements the infant SL Y-connector. However, in this case a port is added to the top of the Y-connector directly above the ETT for the delivery of the aerosol (Fig. 1c). With this configuration, hygroscopic growth of EEG particles is likely delayed until just before entering the ETT. Furthermore, the delivery port allows the aerosol to be correctly positioned in the flow stream in order to reduce deposition in the ETT, which remained consistently high in the study of Longest *et al.* (7).

The transport and deposition of multiple aerosols is considered for the three delivery systems. For a control case, a previously measured aerosol from a mesh nebulizer is considered. To provide the best possible performance of the control, the Aeroneb Lab mesh nebulizer (Aerogen Limited, Galway, Ireland) is employed, which is known to produce a smaller aerosol than the frequently employed Aeroneb Pro device (27). The mesh nebulizer was operated with a 0.2% w/v solution of AS in deionized water. For size determination, the Aeroneb Lab device was placed in a neonatal T-connector, humid air was passed through the device at approximately 5 LPM, and the aerosol along with humidified makeup air was passed through an Andersen Cascade Impactor (ACI; Graseby-Andersen Inc., Smyrna, GA) (7). The measured aerosol MMAD was 4.9 μm with a bimodal distribution characterized by 30% of the aerosol above a droplet diameter of 6 μm (7). The control aerosol case was compared with three different dry particle aerosols with smaller discrete phase diameters as described in Table I. The first of these dry powder aerosols had a geometric diameter of 0.9 μm and was composed of AS model submicrometer particles without hygroscopic excipients. The remaining two aerosols

Table I Aerosol Characteristics for Single Component and Multicomponent Particles and Droplets at the Point of Delivery into the Flow Field

Geometric diameter (μm)	Components and form	Density (kg/m^3)	MMAD (μm)	Polydisperse/ Monodisperse
4.9	0.2% AS droplets	1,000	4.9	Polydisperse
0.9	100% AS particles	1,340	1.04	Monodisperse
0.9	AS:NaCl (50:50) particles	1,650	1.16	Monodisperse
1.8	AS:NaCl (50:50) particles	1,650	2.3	Monodisperse

implemented EEG powders composed of a 50:50 combination of AS and NaCl with initial geometric diameters of 0.9 and 1.8 μm. These sizes are smaller than the optimal fixed particle sizes identified by Longest *et al.* (7) for delivery to infants because, with EEG, water uptake and droplet size increase are expected within the airways due to the inclusion of the hygroscopic excipient.

The effects of aerosol deposition in the commercial and SL Y-connectors were previously analyzed by Longest *et al.* (6,26). In the current study, the aerosols administered to the inspiratory arm of the circuit are initialized in the circular cross section between the inspiratory arm and Y-connector with a parabolic spatial distribution. In contrast, particles delivered to the SL Y-connector with port access are initialized in the 4 mm circular port that is positioned on the top of the Y. The three evaluated delivery systems are referred to as the CM, SL, and SL-port Y-connectors, which are each attached to an identical ETT with a 4 mm ID. Due to the bimodal distribution of the 4.9 μm control aerosol (7), the full initial polydisperse distribution of the aerosol is considered in the simulations. In contrast, dry powder aerosols generated from a mixer-heater (28) or nano-spray dryer (21) and aerosolized with new powder inhalers (22,29,30) are monomodal with relatively small geometric standard deviations (GSD). Therefore, the 0.9 and 1.8 μm dry powder aerosols are initialized as monodisperse in the simulations. Hygroscopic growth of these initially dry powder monodisperse aerosols causes them to take up water, become droplets, and grow in size at different rates forming a polydisperse aerosol with low GSD (25). For the control CM system, only the mesh nebulizer generated droplet aerosol with a 4.9 μm MMAD was considered. All four aerosols (4.9 μm droplets, 0.9 μm AS particles, 0.9 μm AS:NaCl particles, and 1.8 μm AS:NaCl particles) were then evaluated for the SL and SL-port delivery devices.

Infant Physiology

The airway model was representative of a 6-month-old child with an average (50th percentile) weight and height of 8 kg and 67 cm, respectively, based on the CDC growth chart (31). Dimensions of the tracheobronchial (TB) airways were determined from the study of Phalen *et al.* (32), which provides correlations for pediatric airway lengths and diameters based on subject height. The Phalen *et al.* (32) dataset was developed from infant airway cast measurements with ages ranging from 0.03 to 21 years.

The CFD model of the airways was complete through the lobar bronchi based on the measured dimensions of Phalen *et al.* (32) and a typical upper airway bifurcation pattern including curvature of the main bronchi, asymmetrical branching, and out of plane rotation as described by Walenga *et al.* (33) for adults. To simulate aerosol transport and deposition beyond the lobar bronchi, the previously developed stochastic individual path (SIP) modeling approach was employed. Using this method, one branch of each bifurcation is randomly selected for continuation and one branch is ended with an outflow boundary. In the SIP geometry of B4–B15, symmetric bifurcations were assumed with symmetric outflow and successive bifurcations were rotated at 90° around the parent longitudinal axis. Dimensions of the bronchi were again determined from the anatomical cast measurements reported by Phalen *et al.* (32) for the left lower (LL) lobe of a 6-month-old. A single path into each lung lobe was previously shown to represent regional deposition in that lobe (34). Furthermore, the LL lobe was previously found to approximate mean lobar lung deposition in an adult airway model (35). Use of a single lobe in the current study is an approximation. Considering that there are five lung lobes, regional lobar deposition for the entire lung was approximated as the LL lobe value multiplied by a factor of 5.

Ventilation characteristics of the 8 kg newborn infant were based on the recommendations of Walsh *et al.* (36). Time-based parameters were a breathing frequency of 40 br/min, breathing period of 1.5 s, and inspiratory time of 0.5 s. Tidal volume per weight was set to 7 ml/kg, resulting in an inhaled volume of approximately 56 ml. Bias flow and a breath pause were not included. The resulting minute ventilation (breathing frequency times tidal volume) and mean tracheal inspiratory flow were 2.24 and 6.72 LPM, respectively.

The previous study of Longest *et al.* (7) considered cyclic ventilation within a complete lung model of an infant to calculate deposition as well as drug dose exhaled from the ventilation circuit (which never reached the lungs) and dose exhaled from the lungs. By administering the aerosol over the first half of inspiration compared with the entire inspiration time, circuit expired dose was reduced from approximately 30% of the total aerosol to <10% for aerosols in the size range

of 800 nm to 5 μm. Lung expired dose was more dependent on particle size; however, for particles that were approximately 5 μm, the lung expired dose was approximately 5% or less. These values will likely be further reduced with access port aerosol administration, due to a reduced travel distance into the lungs, and for larger tidal volumes. In the current study, the optimal delivery scenario (7) of aerosol administered during approximately the first half of inspiration is applied. Due to port delivery and a larger tidal volume, the administration period is marginally increased to 0.3 s. With port delivery it is envisioned that the aerosol is formed using 3 ml of air delivered over a time period of 0.3 s, which results in a delivery of an additional 0.6 L/min into the flow stream. This is a small additional flow rate compared with the average tracheal flow rate of 6.72 LPM during inspiration. Based the previous estimates described above, expired dose is not predicted in the current study. However, with delivery over the first 0.3 s of inspiration and EEG aerosols that increase in size to 3–5 μm, total expired dose is expected to be less than 15% (7).

Simulations of steady state airflow were conducted through the geometry beginning with the 10 mm diameter inspiratory air line of the ventilator circuit and continuing to the exit of the B15 bifurcation in the infant LL lobe. Inlet conditions for the inspiratory arm of the circuit and aerosol delivery port are summarized in Table II. To capture inspiratory transport, the mean tracheal inlet flow rate of 6.72 LPM was implemented. The inspiratory air was fully humidified with RH = 100% and warmed to 37°C, which represents conditions downstream of the humidifier in the ventilation circuit. Walls of the ventilation circuit, ETT, and airways were also assumed to be wet (RH = 100%) and at body temperature (37°C). For administration of the aerosol in the SL port device, it is envisioned that an active dry powder inhaler will be implemented using a syringe containing ambient room air. Therefore, air delivered through the aerosol delivery port has an RH = 50% and temperature of 25°C. As the air surrounding the aerosol delivered from the port mixes with humid air from the inspiratory line, growth of the hygroscopic powders begins. Timing of this growth is important such that the aerosol can move through the ETT with minimal deposition and then significantly increase in size in the lungs to ensure deposition and prevent exhalation of the drug.

Table II Inlet Conditions for All Systems

	Flow rate (L/min)	Temperature (°C)	Relative humidity
Inspiratory line	6.72	37	100%
Delivery port	0.6	25	50%

Flow Field Solution

A CFD model was implemented that can accurately simulate local temperature and humidity fields, together with droplet trajectories, size change, and deposition within the ventilation circuit and TB model during aerosol delivery. To effectively address both laminar and turbulent flow conditions, a low Reynolds number (LRN) k-ω turbulence model was selected (37). This model has previously been well tested and found to provide good estimates of aerosol transport and deposition in airway models provided that near-wall corrections are included (38–42). To evaluate the variable temperature and RH fields in the conducting airway geometry, interconnected relations governing the transport of heat and mass (water vapor) were also included. These governing equations were presented in detail by Longest and Xi (43) and Longest *et al.* (44).

Particle Transport

To model droplet trajectories, growth, and deposition, a previously developed and tested combination of a commercial code (ANSYS Fluent 12, ANSYS Inc.) and user functions was implemented. User routines were employed to better model near-wall conditions and to simulate multicomponent aerosol condensation and evaporation in the complex three-dimensional temperature and humidity fields. Previous studies have shown that the isotropic turbulence approximation, which is assumed with the LRN k-ω model, can over predict aerosol deposition (45). As a result, a user routine was employed to account for anisotropic near-wall turbulence, as described by Longest *et al.* (44). Other additions to the particle tracking model included (i) a correction to better predict the Brownian motion of submicrometer aerosols and (ii) improved near-wall interpolation of fluid velocities (46).

A user routine was employed to model interconnected droplet temperature and size change resulting from condensation and evaporation. This droplet model accounts for the Kelvin effect, hygroscopicity arising from multiple soluble components, and the effect of droplet temperature on surface vapor pressure (18,25,47). In simulating aerosol evaporation and growth, the effect of the droplets on the continuous phase was neglected, resulting in a one-way coupled approach. One-way coupled simulations are expected to be accurate in this study due to the use of submicrometer aerosols and wetted walls (25).

The deposition efficiency (DE) of particles in the alveolar region was established using the approximation of sedimentation in an inclined tube with a fully developed laminar profile (Poiseuille flow). The Poiseuille flow approximation was selected because it provided a conservatively low estimate of

alveolar deposition compared to the plug flow approximation and was used to define alveolar DE as (48,49)

$$DE_{alveolar} = \frac{2}{\pi}\left[2\kappa\sqrt{1-\kappa^{2/3}} - \kappa^{1/3}\sqrt{1-\kappa^{2/3}} + \arcsin\left(\kappa^{1/3}\right)\right] \quad (1)$$

$$\text{where} \quad \kappa = \frac{3}{4}\frac{v_{settling}}{D}t_{res}\cos\theta. \quad (2)$$

In the expression for κ, D is the tubular geometry diameter, t_{res} is the time that the particles spend in the geometry, θ is the angle relative to the horizontal plane, and the setting velocity is defined as

$$v_{settling} = \rho_{droplet} g d^2/18\mu. \quad (3)$$

Terms in the $v_{settling}$ expression are the droplet density ($\rho_{droplet}$), acceleration due to gravity (g), droplet diameter (d), and absolute viscosity of air (μ). The diameter of alveolar ducts varies by a large amount between the inner flow passage diameter and the outer diameter that includes the airspace added by the attached alveoli. In this study, a value of 0.3 mm was selected for the approximate diameter of infant alveolar ducts and sacs based on the studies of Hofmann *et al.* (50) and Dunnill (51). The alveolar residence time was equal to the time spent in the alveolar airway evaluated as the mean time to reach the exit of the TB airways ($t_{B15\ exit}$), from CFD estimates, subtracted from the total inhalation time (0.5 s) as follows

$$t_{res} = 2(0.5 - t_{\text{B15 exit}}) \quad (4)$$

A factor of 2 was applied to t_{res} to account for the fact that airborne particles or droplets remained in the alveolar airspace an approximately equal amount of time during the inhalation phase and the beginning of the following exhalation phase. Times to reach the alveolar airways ($t_{B15\ exit}$) for the CM, SL, and SL-port devices were approximately 0.1, 0.1, and 0.075 s, respectively. As implemented by Heyder and Gebhart (48) and described by Finlay (49), Eq. (1) was implemented to capture the alveolar deposition fraction including a inclined tube angle of $\theta = 38.24°$, which provides a statistical average of all possible alveolar duct angles in the airways. Once DE of the droplets in the alveolar region is calculated, the alveolar DF is calculated as

$$DF_{alveolar} = DE_{alveolar} \cdot FR \quad (5)$$

where FR is the fraction of the inhaled aerosol (initial drug mass) remaining at the exit of bifurcation B15.

Numerical Methods

In performing the CFD simulations, previously established best-practices were implemented to provide a high quality solution (41). To solve the transport governing equations, the CFD package ANSYS Fluent 12.0, (ANSYS Inc.) coupled with user-defined functions was employed. All transport equations were discretized to be at least second order accurate in space. For the convective terms, a third order QUICK scheme was used to interpolate values from cell centers to nodes. The diffusion terms were discretized using central differences. The outer iteration procedure was stopped when the global mass residual had been reduced from its original value by five orders of magnitude and when the residual-reduction-rates for both mass and momentum were sufficiently small. To ensure that a converged solution had been reached, residual and reduction rate factors were decreased by an order of magnitude and the results were compared. The stricter convergence criteria produced a negligible effect on both velocity and particle deposition fields. To improve accuracy, all calculations were performed in double precision.

The computational meshes in the ventilation circuit region for the CM, SL, and SL-port geometries contained 600k, 610k, and 680k elements, respectively. These computational meshes consisted of hexahedral cells except for the port inlet geometry of the SL-port configuration, which required tetrahedral cells for effective mesh construction. Computational meshes of the upper TB geometry and SIP model consisted of 320k and 880k hexahedral control volumes, respectively. Mesh construction software ICEM and Gambit 2.4 (ANSYS, Inc.) were used to build the grids. Grid density was increased near the walls of all regions. Grid converged results based on negligible change in the velocity and water vapor concentration fields (<1%), as well as negligible differences in the total deposition fractions (<3%), were established for a mesh consisting of approximately 30% fewer control volumes. In order to produce convergent aerosol deposition results, 9k initially monodisperse particles were delivered at the aerosol inlet for each case considered. To improve numerical efficiency and accuracy, the SIP geometry was divided into segments B4–B7 and B8–B15. Flow fields were interpolated between the upstream outlets and the inlets of each of these sections. 90k particles were delivered at the inlet of the SIP section. The MMAD of the polydisperse distributions of the upstream outlets were used to define particle deliveries at the inlet of each SIP section including local droplet water and solute mass fractions, density, and hygroscopic properties. Mass median aerodynamic diameters after growth were calculated based on the midpoint diameters of a standard Andersen Cascade Impactor (52). Doubling the number of droplets considered had a negligible impact on both total and sectional deposition results for all model sections considered.

Validation Case Studies

The CFD model implemented in this study for particle transport, growth, and deposition has been extensively developed and validated compared with *in vitro* drug deposition data using pharmaceutical aerosols. Considering deposition in ventilator components including infant ETTs, CFD model predictions matched *in vitro* deposition results for three different aerosol sizes within the reported experimental standard deviations in almost all cases (6). The CFD model also accurately predicted the deposition of both conventional droplet aerosols and EEG particles with growth compared with *in vitro* experiments in models of orally administered spray aerosols (20) and nasally administered aerosols from a mesh nebulizer (23). The study of Longest *et al.* (25) compared CFD predictions and *in vitro* results of aerosol growth in a coiled tube geometry used to produce a 2 s residence time under lung airway thermodynamic conditions. CFD results of size increase matched the *in vitro* predictions to within 10% and highlighted a gradual and steady size increase of the aerosol droplets. One-way coupled solutions, where the aerosol does not affect the gas phase, were shown to be accurate for realistic pharmaceutical aerosols through a final MMAD of approximately 3 μm. Beyond 3 μm, two-way coupling effects began to gradually appear for the coiled tube geometry setup (25), which had an internal diameter of 22 mm. However, due to smaller air passages in the lower lung, Tian *et al.* (24) demonstrated that two-way coupling was not significant (<10% effect on diameter) for final aerosol sizes approaching 5 μm.

RESULTS AND DISCUSSION

Flow Field Characteristics

Contours of velocity magnitude and velocity vectors on selected planes in the Y-connectors, ETT and airway model are illustrated in Fig. 2. As described previously (7), significant flow disruption occurs in the CM Y-connector, which is illustrated by the unaligned velocity vectors in the expanded view of this region (Fig. 2a). In contrast, the SL designs provide a smooth connection between the inspiratory line and ETT, which reduces flow disruption and results in aligned velocity vectors and gradual changes in flow direction (Fig. 2b and c). Including the aerosol delivery port (Fig. 2c) is observed to result in little additional flow disruption compared to the base SL design (Fig. 2b). In the TB region, the presence of the 4 mm ID ETT results in a jet of airflow that strikes the main carina, likely leading to particle impaction, and is then dispersed (Fig. 2d). In contrast, previous simulations of the naturally occurring laryngeal jet without an ETT indicate that the jet structure attaches to the tracheal walls before reaching the main carina (40). Contours within the bifurcating respiratory geometry illustrate reduced flow velocities as the flow rate is decreased by a factor of 2 with each bifurcation. As the velocity is reduced in each successive bifurcation beyond B3, particle residence time is increased allowing more time for aerosol hygroscopic growth and an increased probability for deposition by impaction and sedimentation.

Relative humidity contours are provided in Fig. 3 for the SL Y-connector with port geometry. As described in Table II, flow enters from the inspiratory line at 100% RH and 6.72 LPM, and flow from the delivery port has an RH of 50% with a flow rate of 0.6 LPM. Wall conditions were 100% RH and 37°C throughout. The delivery port airflow is observed to reduce the RH of the combined flow stream in the vicinity of the Y-connector, which delays the size increase of the aerosol. However, the flow quickly returns to 100% RH within the ETT due to the wet wall condition and larger flow rate from the inspiratory line. The delay in aerosol growth associated with powder administration through the delivery port may reduce depositional losses in the ETT. In contrast, when the aerosol is introduced into the inspiratory line growth occurs throughout the Y-geometry, which will most likely increase the deposition in the connector and ETT.

Aerosol Size Change

The MMAD of the evolving aerosols is provided at the exit of three airway regions in Table III. In the case of the nebulized droplets with an initial diameter of 4.9 μm, the initial aerosol was simulated as polydisperse due to a bimodal particle distribution. This significantly increased its deposition within the Y-connector and ETT resulting in a lower MMAD entering the airways. The resulting MMADs at the exit of B3 (end of the upper TB model) are reported in Table III and the particle distributions were observed to be monomodal at this location. Due to the low concentration of drug (0.2%) in the nebulized droplets and 100% RH in the remainder of the geometry, the MMAD of the nebulized droplets was then held constant during transport through the rest of the lungs. In all other cases, size evolution of the aerosols was simulated due to condensational growth throughout the TB airways. Considering the particles composed of AS and AS:NaCl, significant size increase is observed at the exit of B3 with diameter growth ratios, defined by the current MMAD divided by the initial geometric diameter (d_{geo}), of 2 or more (Table III). Inclusion of the hygroscopic excipient and use of a larger initial particle size clearly increase the aerosol size at the exit of B3. Similarly, the size of all powder aerosols increased with progression through the airways. For the SL-port geometry, trends in growth are similar to those with the SL design. Overall, the aerosol size is smaller with the SL-port case at all locations compared to the SL case due to a reduced exposure time of the aerosol to high humidity associated with

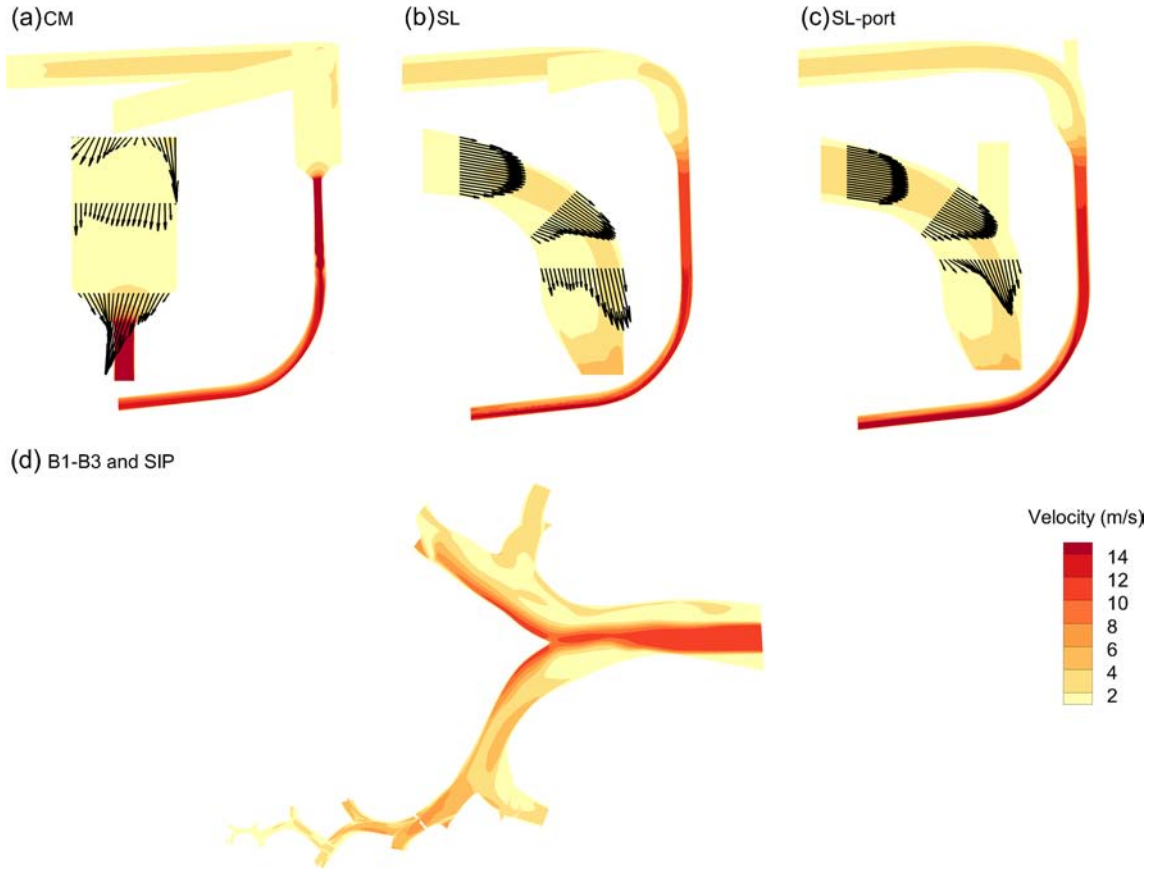

Fig. 2 Contours of velocity magnitude and velocity vectors on selected planes for the (**a**) CM, (**b**) SL, and (**c**) SL-port geometries; as well as (**d**) velocity contours in the upper TB and the LL lobe SIP model for the SL system at steady state inhalation conditions.

the location of aerosol delivery. These reduced aerosol sizes with port delivery are expected to decrease deposition in the ETT and increase deposition in the lower airways and alveolar region.

Particle trajectories contoured by local droplet size in the SL-port design and either AS (d_{geo}=0.9 μm initial size) or AS:NaCl (d_{geo}=1.8 μm) aerosols are displayed in Fig. 4. As predicted by Longest and Hindle (18), some growth is observed for the case of AS alone with a final aerosol size exiting B15 of approximately 2 μm. This is due to the hygroscopic nature of AS, which has a hygroscopic parameter of 4.9 (18).

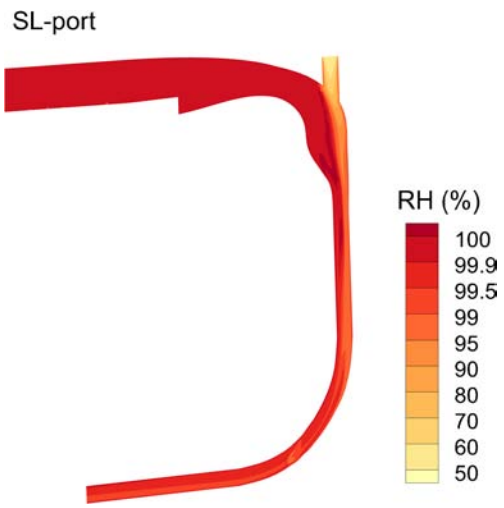

Fig. 3 Contours of relative humidity (*RH*) on selected planes for the SL-port system at steady state inhalation conditions.

Table III Mass Median Aerodynamic Diameter (MMAD) of the Aerosol at the Exit of Various Geometric Regions for All Device and Particle (or Droplet) Combinations

	$MMAD_{B3}$ (μm)	$MMAD_{B7}$ (μm)	$MMAD_{B15}$ (μm)
CM			
4.9 μm AS	2.48	2.48	2.48
SL			
0.9 μm AS	1.80	2.10	2.40
0.9 μm AS:NaCl	2.65	3.54	4.35
1.8 μm AS:NaCl	4.0	4.97	5.79
4.9 μm AS	2.72	2.72	2.72
SL-port			
0.9 μm AS	1.53	1.80	2.07
0.9 μm AS:NaCl	2.19	3.05	3.90
1.8 μm AS:NaCl	3.35	4.25	4.96
4.9 μm AS	2.28	2.28	2.28

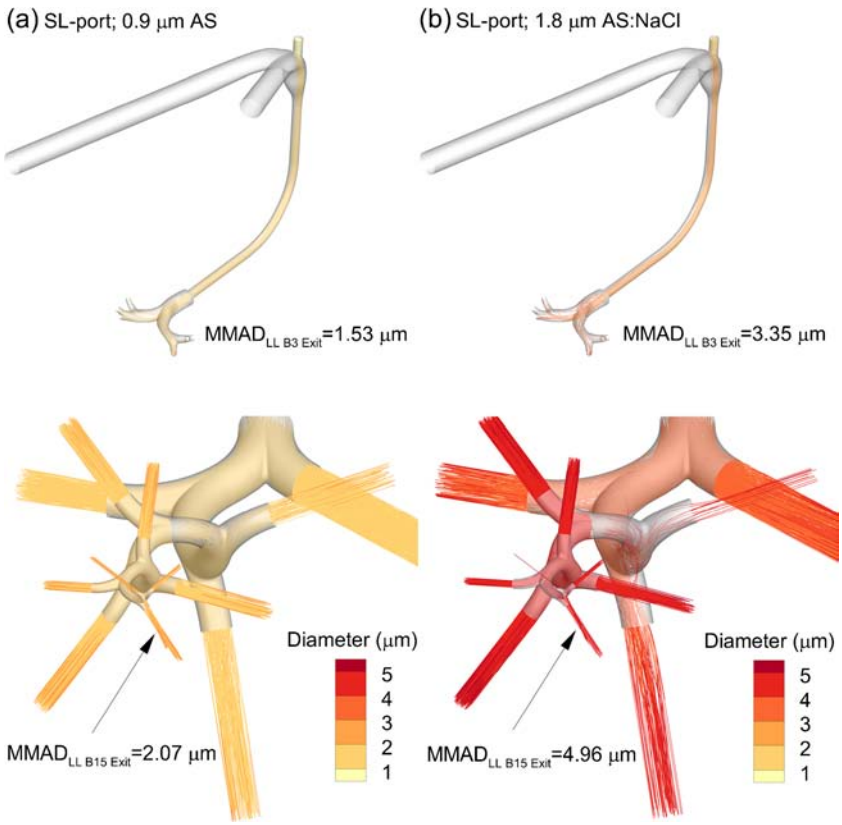

Fig. 4 Droplet trajectories colored according to diameter in the SL-port system and TB geometries for initially monodisperse (**a**) 900 nm AS (minimum growth) and (**b**) 1.8 μm combination particles of AS:NaCl (maximum growth).

However, addition of the hygroscopic excipient provides a large increase in the aerosol size exiting B3 and B15, where MMADs at both of these locations are more than two times greater than with AS alone. In comparison to AS, NaCl has a hygroscopic parameter of 77.9 (18), indicating a significantly larger potential for hygroscopic growth. Both the Stokes number and settling velocity of the aerosols are proportional to the droplet diameter squared. As a result, increasing the droplet diameter by a factor of 2 will result in even larger increases in deposition due to impaction and sedimentation in the airway model.

Aerosol Deposition

Deposition of the nebulized 4.9 μm aerosol is illustrated with the three delivery systems in Fig. 5. As demonstrated by Longest *et al.* (7), the SL infant configuration significantly reduces deposition in the Y-connector (14.1% *vs.* 23.7%). With the newly proposed delivery port design, depositional loss in the SL Y-connector is nearly eliminated (DF < 0.9%). However, reductions in Y-connector deposition result in higher delivery and deposition fractions in the ETT. Nevertheless, the SL designs still increase deposition fraction in the airways compared to the CM design. Fractions remaining at the exit of B15 and delivery to the alveolar region are similar with a slightly lower value for the SL-port design due to the increased combined flow rate and resulting higher net TB deposition.

Device deposition for all aerosols considered is reported in Table IV. For the SL design, the 0.9 μm EEG aerosols did not largely increase deposition compared to the 0.9 μm AS aerosol in the device (15.8% *vs.* 13.7%), which indicates that excessive growth has not occurred in the ETT. Compared with the 4.9 μm droplet aerosol in the SL design, the 0.9 μm EEG aerosol reduced device deposition by a factor of 3x and the 1.8 μm reduced device deposition by a factor of 2x. The SL-port geometry provided further reduction in device deposition. With the EEG aerosols, the SL-port device produced total depositional losses of 4.3–7.8%, which was a factor of 4–5x lower than with the SL configuration.

For the 1.8 μm EEG aerosol, Fig. 6 compares regional deposition between the SL and SL-port devices. The SL-port design is observed to reduce depositional loss by an order of magnitude in the Y-geometry and a factor of 2-fold in the ETT compared with the SL connector. This reduction is due to the smaller aerosol sizes in the ETT associated with the port administration and delayed condensational growth. Because the aerosol is smaller in the upper airways with the port device, deposition is also lower in the upper TB region of B1–B3 (27.3% *vs.* 36.7%; Fig. 6). However, deposition is then equal between the devices in the mid-TB level of B4–B7 (~16%) and higher with the port device in B8–B15 (4.7% *vs.* 2.8%). As a result, the port device appears to waste less

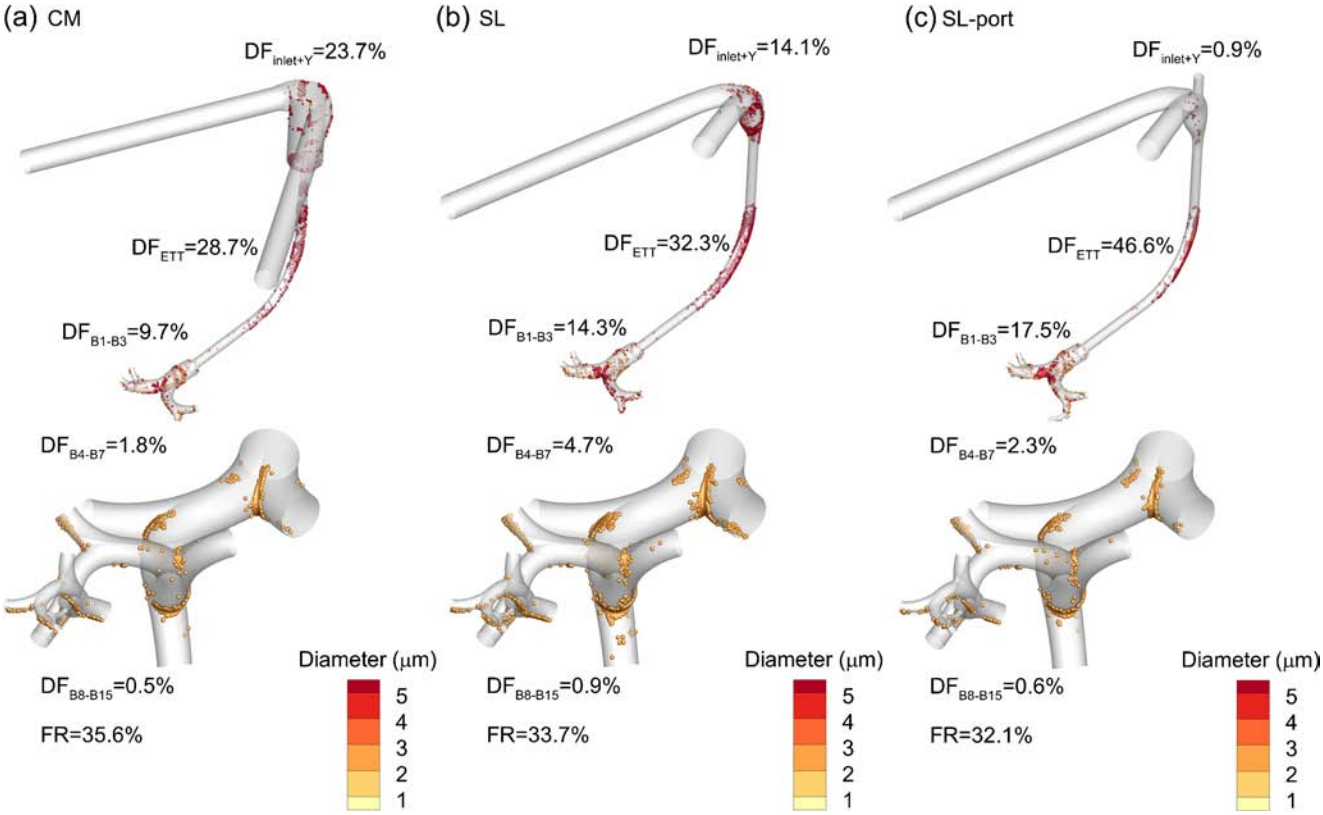

Fig. 5 Particle deposition locations and regional DFs for initially polydisperse particles (MMAD = 4.9 μm) in the (**a**) CM, (**b**) SL, and (**c**) SL-port systems.

medication in the Y-geometry and ETT, and shifts deposition toward the more distal airways and alveolar region. This effect is largely due to administering the aerosol within the Y-geometry such that growth is delayed and the aerosol has a smaller size in the ETT and upper TB airways.

Deposition fractions of the aerosol as a percentage of aerosolized dose are provided for all cases in Table V

Table IV CFD Predictions of Drug Deposition Fraction (DF) in the Device as a Percentage of the Aerosolized Dose for All Delivery System and Particle (or Droplet) Combinations.

Aerosols	$DF_{inlet+Y}$	DF_{ETT}	$DF_{Total\ device}$
CM			
4.9 μm AS	23.7	28.7	52.4
SL			
0.9 μm AS	9.4	4.3	13.7
0.9 μm AS:NaCl	9.7	6.1	15.8
1.8 μm AS:NaCl	12.4	14.5	26.9
4.9 μm AS	14.1	32.3	46.4
SL-port			
0.9 μm AS	0.7	2.8	3.5
0.9 μm AS:NaCl	0.7	3.6	4.3
1.8 μm AS:NaCl	0.8	7.0	7.8
4.9 μm AS	0.9	46.6	47.5

including FR at the exit of B15 and the associated DF in the alveolar region. Lung DF is the sum of total TB (DF_{TB}) and alveolar ($DF_{alveolar}$) deposition. The aerosol fraction that is not deposited, which is the difference between the FR and $DF_{alveolar}$, may be exhaled or may be deposited in the TB region during exhalation. However, the model does not currently account for TB deposition during exhalation. It is noted that differences between the FR and $DF_{alveolar}$ only occur for the cases that are not EEG aerosols. For the case of 4.9 μm initial droplets, this difference is approximately 15%.

Maximum deposition fraction in the TB region was 55.7%, which was provided by the SL device and the 1.8 μm AS:NaCl EEG aerosol. This value was 4–5 fold greater than the CM delivery system with a nebulized aerosol. Maximum fractions remaining and delivered to the alveolar region were 66–80% provided by the 0.9 μm AS aerosol, due to the combination of low device and low TB deposition. However, predictions of alveolar deposition using Eq. (1) for the 0.9 μm AS aerosol (not including a hygroscopic excipient) were approximately 25% indicating a high fraction of the aerosol was likely exhaled with the implemented tidal breathing waveform. In contrast, the 0.9 μm EEG aerosol with both delivery devices penetrated to the alveolar region at a high fraction and had sufficient size to fully deposit during the available time. As a result, the maximum alveolar deposition fraction was approximately 68% provided by the SL-port

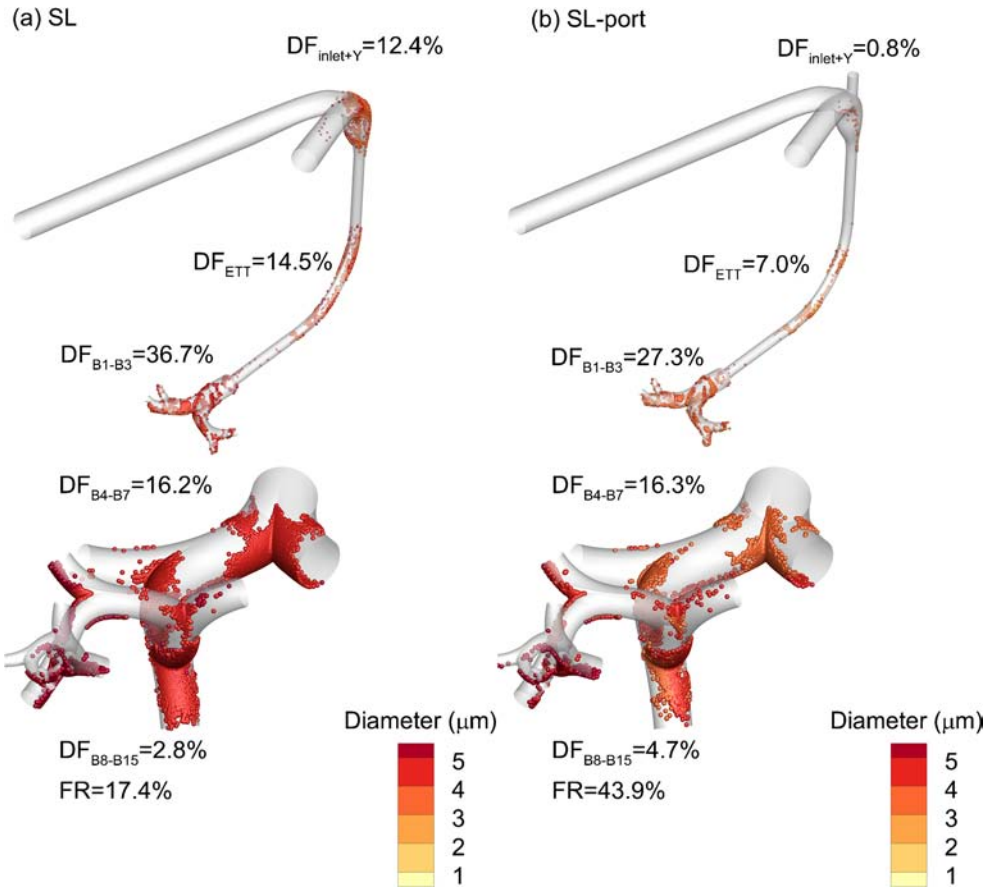

Fig. 6 Particle deposition locations and regional DFs for 1.8 μm combination particles of AS:NaCl in the (**a**) SL and (**b**) SL-port systems.

delivery approach and 0.9 μm EEG aerosol. Considering total lung deposition fraction, the 0.9 μm EEG aerosols provided maximum values of 84.2 and 95.7% for the SL and SL-port devices, respectively. It is noted that these predictions include evaluation of residence time in the TB and alveolar airways. To implement Eq. (1), alveolar residence times in the TB region were predicted from the CFD model as described in the Methods. Use of these single average residence times for each system is an approximation compared with simulating the individual residence times of every particle in the TB and alveolar airways. Moreover, particles near the walls may have higher residence times thereby reducing the FR that is assumed to enter the alveolar airways.

As described by Longest *et al.* (7), the exhalation of aerosol dose remaining in the device and TB airways can be very large with infants. The study of Longest *et al.* (7) implemented

Table V CFD Predictions of Drug Deposition Fraction (DF) in the Lungs as a Percentage of Aerosolized Dose for All Delivery System and Particle (or Droplet) Combinations. Regional Predictions Include the Total TB Deposition (DF_{TB}), Fraction of Aerosol Remaining (FR) at the Exit of B15 (Inlet of the Alveolar Region), Total Alveolar Deposition ($DF_{alveolar}$), and Total Lung Deposition (DF_{lung}).

Aerosols	$DF_{B1–B3}$	$DF_{B4–B7}$	$DF_{B8–B15}$	DF_{TB}	FR	$DF_{alveolar}$	DF_{lung}
CM							
4.9 μm AS	9.7	1.8	0.5	12.0	35.6	14.9	26.9
SL							
0.9 μm AS	17.7	1.4	1.1	20.2	66.1	25.5	45.7
0.9 μm AS:NaCl	22.8	8.7	3.5	35.0	49.2	49.2	84.2
1.8 μm AS:NaCl	36.7	16.2	2.8	55.7	17.4	17.4	73.1
4.9 μm AS	14.3	4.7	0.9	19.9	33.7	16.6	36.5
SL-port							
0.9 μm AS	13.8	1.0	0.8	15.6	80.9	25.7	41.3
0.9 μm AS:NaCl	18.9	6.6	2.6	28.1	67.6	67.6	95.7
1.8 μm AS:NaCl	27.3	16.3	4.7	48.3	43.9	43.9	92.2
4.9 μm AS	17.5	2.3	0.6	20.4	32.1	11.7	32.1

delivery during the first half of inspiratory flow to reduce the circuit exhaled dose by a factor of approximately 3-fold and increase the lung dose by 2-fold compared with dose delivered over the entire inhalation cycle. In the current study, lung exhaled dose is reduced due to the close proximity of the delivery port to the ETT, increase in aerosol size in the lungs, and larger inhaled volume associated with patient age compared to Longest *et al.* (7). Still, lung exhaled doses of 5–10% may occur due to some aerosolized droplets remaining in the device and TB airways, which are not captured by the current CFD model.

Trends in regional and total TB deposition fraction are illustrated in Fig. 7 for the CM device *vs.* the SL and SL-port geometries. For the commercial device, a majority of the aerosol is deposited in the Y-connector and ETT with a small fraction in the airways. This trend is reversed with both SL designs and powder aerosols with a small amount of loss in the device and a majority of the aerosol depositing in the lungs. Considering TB deposition fraction and the SL designs, delivery with the 0.9 μm AS powder aerosols is nearly equal to delivery with the 4.9 μm nebulized droplets. This is because the nebulized droplet aerosol decreases in size entering the lungs and the submicrometer particles increase in size such that both aerosols are near 2 μm entering the alveolar airspace. The 0.9 μm AS aerosol also has significantly less device deposition than the 4.9 μm nebulized aerosol. For EEG aerosols, the larger initial size particles increase regional and total TB deposition fraction with only a small increase in total device deposition. However, if initial size is increased further, higher device losses will start to diminish lung delivered dose.

Trends in alveolar and total lung deposition fraction are displayed in Fig. 8 with the addition of an experimentally generated aerosol administered with the SL Y-connector from the study of Longest *et al.* (7). In this previous study, a new mixer-heater device was used to generate and deliver an aerosol with a MMAD = 1.78 μm directly to the inspiratory arm of the SL Y-connector (without a port) over the first half of the inspiratory period. The aerosol was composed of dried AS particles and did not contain a hygroscopic excipient. The system flow rate was 5 LPM and a 3 mm ID ETT was considered for the delivery of aerosols to a newborn infant. As displayed in Fig. 8, the resulting lung delivery rate was greater than 40%.

As described in the Introduction, previous studies have reported lung delivery efficiencies with mesh nebulizers of approximately 10% for infants. Lung deposition predictions of approximately 30% with the CM system and current simulations (Fig. 8) are likely due to the use of the Aeroneb Lab nebulizer, which produces a smaller aerosol than the commercial mesh nebulizers used in previous studies, and exclusion of the exhaled dose from the device and lung, which were shown to result in approximately 30–40% aerosol losses when synchronization with inspiratory flow was not employed (7). Furthermore, the current study also excluded the infant T-connector, which was previously shown to result in an additional 40% loss of the aerosol (26). Use of the SL design with the mesh nebulizer 4.9 μm aerosol increases the lung dose to approximately 40%, but is also subject to reductions in delivered dose associated with continuous nebulization and inclusion of the infant T-connector. Results with the 1.78 μm aerosol from the study of Longest *et al.* (7) cannot be directly compared with the results of the current study, because these systems were based on different size ETTs and different flow rates. However, the lung deposition fraction from this previous study is similar to values provided with the 0.9 μm AS aerosol and nebulized droplets with the SL models. In contrast, lung deposition fraction with the EEG approach appears significantly higher with values in the range of 70–85% for the SL device and 90–95% for the SL-port device. As with Longest *et al.* (7), each of these high delivered doses will require administration of the aerosol over the first half of inhalation to avoid large exhaled doses from the device and upper TB airways.

Limitations of the current study include the assumption that LL lobe deposition fraction is a representative average of all airway lobes, the exclusion of ventilator bias flow, and

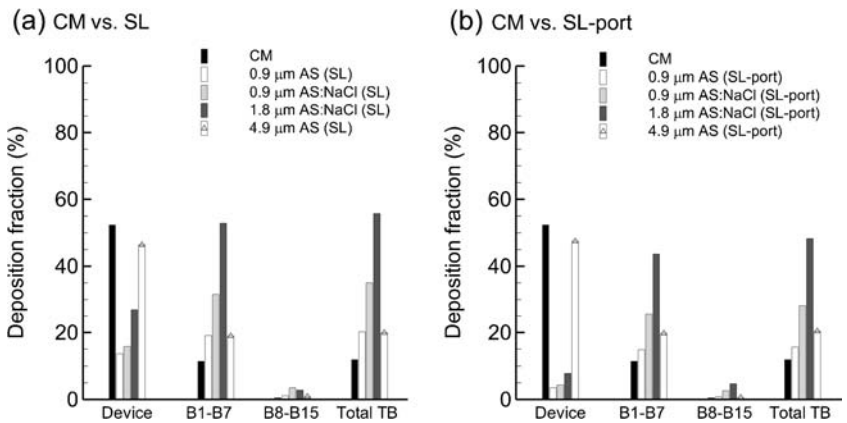

Fig. 7 Predictions of DFs in the device and TB regions for (**a**) CM *vs.* SL and (**b**) CM *vs.* SL-port delivery.

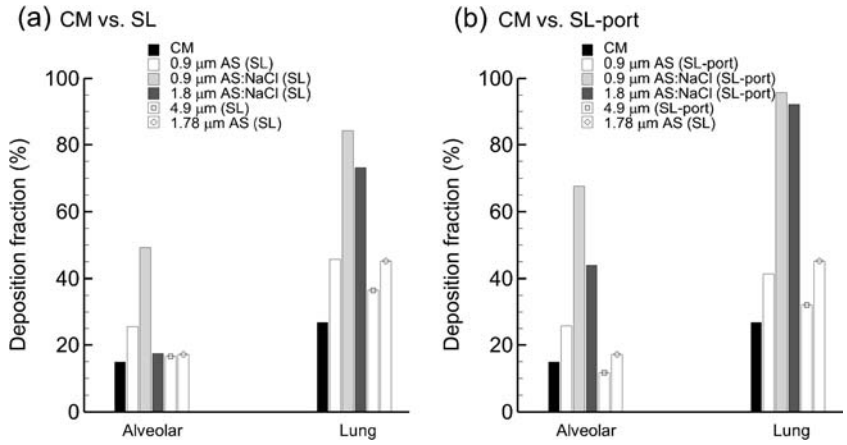

Fig. 8 Predictions of DFs in the alveolar regions and total lung for (**a**) CM *vs.* SL and (**b**) CM *vs.* SL-port delivery.

estimates of exhaled dose based on a previous study. As described, the assumption regarding LL lobe dose was based on a standing adult (35), which may not be applicable to ventilated infants. Some previous studies on the delivery of aerosols to ventilated infants have included a ventilator bias flow (13). Furthermore, exhaled dose will reduce the predicted lung deposition fractions (7). However, it is estimated that these limitations will not largely affect the deposition fraction predictions and the relative comparison of the delivery systems.

A number of parameters were held constant in the current study that could have an effect on regional deposition characteristics within the lungs. For example, results are based on fixed ventilation parameters, a constant initial hygroscopic excipient loading and a single hygroscopic excipient material. The effect of varying these parameters on regional deposition fractions should be explored. However, consistently high delivery efficiency to the lungs is expected based on the use of initially small particles and the observed rate of droplet size growth (Fig. 4).

In this study, AS was selected as a model drug and NaCl was the only hygroscopic excipient that was considered. The EEG aerosols were observed to achieve large increases in TB and total lung deposition fractions. Compared with conventional aerosols, EEG provides increases in upper and lower TB deposition fractions (Fig. 7) with maximum deposited dose in the upper TB airways (B1–B7). This targeted deposition of the dose aligns with the expected receptor locations for a bronchodilator like AS, based on airway response to particles of different sizes in adults (53). However, the EEG approach also increases the alveolar delivered dose. Increases in total lung dose and alveolar exposure should be considered when administering EEG aerosols and the total dose should be adjusted appropriately. In contrast with AS, a number of existing and new inhaled medications are intended for alveolar delivery. Examples of alveolar targeted inhaled medications include aerosolized surfactants and antibiotics. These medications can be effectively deposited in the alveolar region using an EEG approach by adjusting the initial particle size, hygroscopic excipient type, and hygroscopic excipient loading as described in previous studies with adult airways (18,19,24).

CONCLUSIONS

In conclusion, EEG powder aerosols were compared with a mesh nebulized droplet aerosol in CM and SL Y-connectors, an ETT, and a lung model. Use of the SL configuration (without a port) with EEG powder aerosols reduced total device depositional loss with the CM system of 52.4% to a minimum value of 15.8%. The SL configuration maximized TB deposition fraction with a value of 55.7% compared to the CM system value of 12%. Employing the aerosol delivery port on the SL configuration provided several additional key advantages related to the associated delay in EEG particle growth. With the port design and EEG aerosols, the CM system depositional loss of 52.4% was further reduced to <10% (1.8 μm AS:NaCl) with a minimum value of <5% (0.9 μm AS:NaCl). The SL-port configuration also shifted the lung deposition toward the lower TB airways and provided the maximum observed alveolar deposition fraction (67.6%) and total lung deposition fraction (95.7%), both achieved with the initial 0.9 μm AS:NaCl aerosol. These predictions include cyclic breathing in the alveolar region. Due to hygroscopic growth, all EEG droplets reaching the alveolar region were fully deposited, *i.e.*, DE in the alveolar region was 100%. However, minimizing exhaled dose from the TB airways and delivery system requires delivering the dose over the first half of inhalation. As demonstrated by Longest *et al.* (7) for an infant model, a majority of the drug dose of particles in the size range of <2 μm is lost due to exhalation with tidal infant breathing. The combination of EEG aerosols and port delivery, which reduces the distance to the lungs and increases the aerosol size once in the lungs, will reduce the exhaled dose fraction. Future studies are required

to develop the devices that can achieve the prescribed delivery of combination EEG aerosols over a fraction of the inhalation time period and test the simulation results with *in vitro* models before testing in animals and humans can begin.

ACKNOWLEDGMENTS AND DISCLOSURES

Research reported in this publication was supported by the Eunice Kennedy Shriver National Institute of Child Health & Human Development of the National Institutes of Health under Award Number R21HD073728. The content is solely the responsibility of the authors and does not necessarily represent the official views of the National Institutes of Health. Dr. Michael Hindle of the VCU Department of Pharmaceutics is gratefully acknowledged for helpful comments on this study and for reviewing the manuscript. No conflicts of interest exist.

REFERENCES

1. Fink JB. Aerosol delivery to ventilated infant and pediatric patients. Respir Care. 2004;49:653–65.
2. Mazela J, Polin RA. Aerosol delivery to ventilated newborn infants: historical challenges and new directions. Eur J Pediatr. 2011;170: 433–44.
3. Rubin BK. Pediatric aerosol therapy: new devices and new drugs. Respir Care. 2011;56:1411–21.
4. Rubin BK, Fink JB. Aerosol therapy for children. Respir Care Clin N Am. 2001;7:175–213.
5. Fok TF, Monkman S, Dolovich M, Gray S, Coates G, Paes B, *et al.* Efficiency of aerosol medication delivery from a metered dose inhaler versus jet nebulizer in infants with bronchopulmonary dysplasia. Pediatr Pulmonol. 1996;21:301–9.
6. Longest PW, Azimi M, Golshahi L, Hindle M. Improving aerosol drug delivery during invasive mechanical ventilation with redesigned components. Respiratory Care. 2014;59:686–8.
7. Longest PW, Azimi M, Hindle M. Optimal delivery of aerosols to infants during mechanical ventilation. J Aerosol Med Pulm Drug Deliv. 2013. doi:10.1089/jamp.2013.1077.
8. Fok TF, Alessa M, Monkman S, Dolovich M, Girard L, Coates G, *et al.* Pulmonary deposition of salbutamol aerosol delivered by metered dose inhaler, jet nebulizer, and ultrasonic nebulizer in mechanically ventilated rabbits. Pediatr Res. 1997;42:721–7.
9. Borgstrom L, Olsson B, Thorsson L. Degree of throat deposition can explain the variability in lung deposition of inhaled drugs. J Aerosol Med. 2006;19:473–83.
10. Dhand R. Inhalation therapy in invasive and noninvasive mechanical ventilation. Curr Opin Crit Care. 2007;13:27–38.
11. Dubus JC, Vecellio L, De Monte M, Fink JB, Grimbert D, Montharu J, *et al.* Aerosol deposition in neonatal ventilation. Pediatr Res. 2005;58:10–4.
12. Sidler-Moix AL, Dolci U, Berger-Gryllaki M, Pannatier A, Cotting J, Di Paolo ER. Albuterol delivery in an in vitro pediatric ventilator lung model: comparison of jet, ultrasonic, and mesh nebulizers. Pediatr Crit Care Med. 2013;14:E98–E102.
13. Ari A, Atalay OT, Harwood R, Sheard MM, Aljamhan EA, Fink JB. Influence of nebulizer type, position, and bias flow on aerosol drug delivery in simulated pediatric and adult lung models during mechanical ventilation. Respir Care. 2010;55:845–51.
14. Mazela J, Chmura K, Kulza M, Henderson C, Gregory TJ, Moskal A, *et al.* Aerosolized albuterol sulfate delivery under neonatal ventilatory conditions: In vitro evaluation of a novel ventilator circuit patient interface connector. J Aerosol Med Pulm Drug Deliv. 2013. doi:10.1089/jamp.2012.0992.
15. Pohlmann G, Iwatschenko P, Koch W, Windt H, Rast M, Gama de Abreu M, *et al.* A novel continuous powder aerosolizer (CPA) for inhalative administration of highly concentrated recombinant surfactant protein-C (rSP-C) surfactant to perterm neonates. J Aerosol Med Pulm Drug Deliv. 2013;26:370–9.
16. Laube BL, Sharpless G, Shermer C, Sullivan V, Powell K. Deposition of dry powder generated by solovent in Sophia Anatomical infant nose-throat (SAINT) model. Aerosol Sci Technol. 2012;46:514–20.
17. Everard ML, Devadason SG, LeSouef PN. In vitro assessment of drug delivery through an endotracheal tube using a dry powder inhaler delivery system. Thorax. 1996;51:75–7.
18. Longest PW, Hindle M. Numerical model to characterize the size increase of combination drug and hygroscopic excipient nanoparticle aerosols. Aerosol Sci Technol. 2011;45:884–99.
19. Hindle M, Longest PW. Condensational growth of combination drug-excipient submicrometer particles for targeted high efficiency pulmonary delivery: evaluation of formulation and delivery device. J Pharm Pharmacol. 2012;64:1254–63.
20. Longest PW, Tian G, Li X, Son Y-J, Hindle M. Performance of combination drug and hygroscopic excipient submicrometer particles from a softmist inhaler in a characteristic model of the airways. Ann Biomed Eng. 2012;40:2596–610.
21. Son Y-J, Longest PW, Hindle M. Aerosolization characteristics of dry powder inhaler formulations for the excipient enhanced growth (EEG) application: effect of spray drying process conditions on aerosol performance. Int J Pharm. 2013;443:137–45.
22. Son Y-J, Longest PW, Tian G, Hindle M. Evaluation and modification of commercial dry powder inhalers for the aerosolization of submicrometer excipient enhanced growth (EEG) formulation. Eur J Pharm Sci. 2013;49:390–9.
23. Golshahi L, Tian G, Azimi M, Son Y-J, Walenga RL, Longest PW, *et al.* The use of condensational growth methods for efficient drug delivery to the lungs during noninvasive ventilation high flow therapy. Pharm Res. 2013;30:2917–30.
24. Tian G, Longest PW, Li X, Hindle M. Targeting aerosol deposition to and within the lung airways using excipient enhanced growth. J Aerosol Med Pulm Drug Deliv. 2013;26:248–65.
25. Longest PW, Hindle M. Condensational growth of combination drug-excipient submicrometer particles: comparison of CFD predictions with experimental results. Pharm Res. 2012;29:707–21.
26. Longest PW, Golshahi L, Hindle M. Improving pharmaceutical aerosol delivery during noninvasive ventilation: effects of streamlined components. Ann Biomed Eng. 2013;41:1217–32.
27. Longest PW, Spence BM, Holbrook LT, Mossi KM, Son Y-J, Hindle M. Production of inhalable submicrometer aerosols from conventional mesh nebulizers for improved respiratory drug delivery. J Aerosol Sci. 2012;51:66–80.
28. Longest PW, Walenga RL, Son Y-J, Hindle M. High efficiency generation and delivery of aerosols through nasal cannula during noninvasive ventilation. J Aerosol Med Pulm Drug Deliv. 2013;26: 266–79.
29. Longest PW, Son Y-J, Holbrook LT, Hindle M. Aerodynamic factors responsible for the deaggregation of carrier-free drug powders to form micrometer and submicrometer aerosols. Pharm Res. 2013;30:1608–27.
30. Behara SRB, Farkas DR, Hindle M, Longest PW. Development of a high efficiency dry powder inhaler: effects of capsule chamber design and inhaler surface modifications. Pharm Res. 2014;31:360–72.
31. National Centers for Health Statistics. Length-for-age and Weight for age percentiles. 2000. http://www.cdc.gov/growthcharts.

32. Phalen RF, Oldham MJ, Beaucage CB, Crocker TT, Mortensen JD. Postnatal enlargement of human tracheobronchial airways and implications for particle deposition. Anat Rec. 1985;212:368–80.
33. Walenga RL, Tian G, Longest PW. Development of characteristic upper tracheobronchial airway models for testing pharmaceutical aerosol delivery. ASME J Biomech Eng. 2013;135(9):091010.
34. Tian G, Longest PW, Su G, Walenga RL, Hindle M. Development of a stochastic individual path (SIP) model for predicting the tracheobronchial deposition of pharmaceutical aerosols: effects of transient inhalation and sampling the airways. J Aerosol Sci. 2011;42:781–99.
35. Longest PW, Tian G, Delvadia R, Hindle M. Development of a stochastic individual path (SIP) model for predicting the deposition of pharmaceutical aerosols: effects of turbulence, polydisperse aerosol size, and evaluation of multiple lung lobes. Aerosol Sci Technol. 2012;46:1271–85.
36. Walsh BK, DiBlasi RM. Mechanical ventilation of the neonate and pediatric patient. In: Walsh BK, Czervinske MP, DiBlasi RM, editors. Perinatal and pediatric respiratory care. St. Louis: Saunders Elsevier; 2010.
37. Wilcox DC. Turbulence modeling for CFD. 2nd ed. California: DCW Industries, Inc.; 1998.
38. Longest PW, Hindle M, Das Choudhuri S, Xi J. Comparison of ambient and spray aerosol deposition in a standard induction port and more realistic mouth-throat geometry. J Aerosol Sci. 2008;39:572–91.
39. Longest PW, Vinchurkar S. Validating CFD predictions of respiratory aerosol deposition: effects of upstream transition and turbulence. J Biomech. 2007;40:305–16.
40. Xi J, Longest PW, Martonen TB. Effects of the laryngeal jet on nano- and microparticle transport and deposition in an approximate model of the upper tracheobronchial airways. J Appl Physiol. 2008;104:1761–77.
41. Longest PW, Holbrook LT. In silico models of aerosol delivery to the respiratory tract - development and applications. Adv Drug Deliv Rev. 2012;64:296–311.
42. Longest PW, Tian G, Walenga RL, Hindle M. Comparing MDI and DPI aerosol deposition using in vitro experiments and a new stochastic individual path (SIP) model of the conducting airways. Pharm Res. 2012;29:1670–88.
43. Longest PW, Xi J. Condensational growth may contribute to the enhanced deposition of cigarette smoke particles in the upper respiratory tract. Aerosol Sci Technol. 2008;42:579–602.
44. Longest PW, Hindle M, Das Choudhuri S, Byron PR. Numerical simulations of capillary aerosol generation: CFD model development and comparisons with experimental data. Aerosol Sci Technol. 2007;41:952–73.
45. Matida EA, Finlay WH, Grgic LB. Improved numerical simulation of aerosol deposition in an idealized mouth-throat. J Aerosol Sci. 2004;35:1–19.
46. Longest PW, Xi J. Effectiveness of direct Lagrangian tracking models for simulating nanoparticle deposition in the upper airways. Aerosol Sci Technol. 2007;41:380–97.
47. Longest PW, Hindle M. CFD simulations of enhanced condensational growth (ECG) applied to respiratory drug delivery with comparisons to in vitro data. J Aerosol Sci. 2010;41:805–20.
48. Heyder J, Gebhart J. Gravitational deposition of particles from laminar aerosol flow through inclined circular tubes. J Aerosol Sci. 1977;8:289–95.
49. Finlay WH. The mechanics of inhaled pharmaceutical aerosols. San Diego: Academic; 2001.
50. Hofmann W, Martonen TB, Graham RC. Predicted deposition of nonhygroscopic aerosols in the human lung as a function of subject age. J Aerosol Med. 1989;2:49–67.
51. Dunnill MS. Postnatal growth of the lung. Thorax. 1962;17:329–33.
52. Vinchurkar S, Longest PW, Peart J. CFD simulations of the Andersen cascade impactor: model development and effects of aerosol charge. J Aerosol Sci. 2009;40:807–22.
53. Usmani OS, Biddiscombe MF, Nightingale JA, Underwood SR, Barnes PJ. Effects of bronchodilator particle size in asthmatic patients using monodisperse aerosols. J Appl Physiol. 2003;95:2106–12.